Published online: 2020-01-09

In Vivo Computed Tomography Direct Volume Rendering of the Anterior Ethmoidal Artery: A Descriptive Anatomical Study

Filippo Cascio[1] Alberto Cacciola[2] Simona Portaro[3] Gianpaolo Antonio Basile[2] Giuseppina Rizzo[2] Andrè Wady Debes Felippu[4] Alexandre Wady Debes Felippu[4] Antongiulio Bruschetta[2] Carmelo Anfuso[3] Felice Cascio[1] Demetrio Milardi[2,3] Alessia Bramanti[3]

[1] Department of Otorhinolaryngology, Papardo Piemonte Reunited Hospitals, Messina, Sicilia, Italy
[2] Department of Biomedical, Odontoiatric, Morphological and Functional Imaging Sciences, Università degli Studi di Messina, Messina, Italy
[3] Scientific Institute for Research, Hospitalization and Health Care Centro Neurolesi Bonino Pulejo, Messina, Italy
[4] Department of Otorhinolaryngology, Instituto Felippu, São Paulo, Brazil

Address for correspondence Prof. Demetrio Milardi, Department of Biomedical, Dental Sciences and Morphological and Functional Images, Univeristy of Messina, Messina, Italy (e-mail: dmilardi@unime.it).

Int Arch Otorhinolaryngol 2020;24:e38–e46.

Abstract

Introduction The clinical relevance of the anatomy and variations of the anterior ethmoidal artery (AEA) is outstanding, considering its role as a landmark in endoscopic surgery, its importance in the therapy of epistaxis, and the high risks related to iatrogenic injuries.

Objective To provide an anatomical description of the course and relationships of the AEA, based on direct computed-tomography (CT)-based 3D volume rendering.

Methods Direct volume rendering was performed on 18 subjects who underwent (CT) with contrast medium for suspected cerebral aneurism.

Results The topographical location of 36 AEAs was assessed as shown: 10 dehiscent (27.8%), 20 intracanal (55.5%), 6 incomplete canals (16.7%). Distances from important topographic landmarks are reported.

Conclusion This work demonstrates that direct 3D volume rendering is a valid imaging technique for a detailed description of the anterior ethmoidal artery thus representing a useful tool for head pre-operatory assessments.

Keywords
- anterior ethmoidal artery
- CT
- volume rendering

Introduction

The anterior ethmoidal artery (AEA), a branch of the ophthalmic artery, crosses three cavities along its course: it arises in the orbit, reaches the ethmoidal labyrinth passing through the bony anterior ethmoidal canal (AEC) together with its homonymous vein and nerve, and finally enters the olfactory fossa, through the lateral lamella of the cribriform plate, along the so-called anterior ethmoidal sulcus,[1] where it becomes the anterior falx artery[2].

Several studies demonstrated that the AEC is not always continuous in its bony structure, but it may show a partial or complete bone dehiscence in its most caudal portion.[1,3,4] Significant intrasubject side-to-side variability may exist so that the bony canal can be complete on one side and partially or completely open on the other one.

Moreover, useful information about the distance of the AEA from the columella,[5] the middle turbinate axilla and the nasal valve[1,6] has been provided.

received
October 25, 2018
accepted
August 18, 2019

DOI https://doi.org/10.1055/s-0039-1698776.
ISSN 1809-9777.

The AEA is one of the most important landmarks in endoscopic surgery, representing a fundamental orientation point for ethmoidal fovea and anterior cranial fossa.[7,8]

In the surgical approach to the frontal recess, the AEC marks its posterior border.[9,10] Likewise, in the external approaches, AEA identification in the fronto-ethmoidal suture marks the ventral limit of the anterior cranial fossa.[11]

In addition to the marking function, the AEA, together with the arteries coming out from the sphenopalatine foramen, plays a key role for vascular ligation in nasal surgery to control epistaxis during endoscopic sinus surgery (ESS).[12,13]

Considering the huge variety of its anatomical localization, course, and length, the preoperative assessment of AEA is of clinical relevance. Indeed, severe iatrogenic injuries may lead to liquor fistulas, intracranial bleeding and blindness, if not decompressed within an hour.[14] As shown by Cassano et al,[12] if a good hemostatic control is performed under endoscopic view during the nasal surgery, the nasal precautionary intraoperative packing is not justifiable, considering the low percentage of postoperative epistaxis. Furthermore, ligation of the sphenopalatine complex and of the AEA is a good way to gain control of epistaxis.[15]

The application of preoperative imaging techniques allows to obtain information about the development of the paranasal sinuses, variants of pneumatization, as well as anatomical variants of the vessels in relation to the adjacent rhino-ethmoidal structures, thus allowing accurate surgical planning and increasing safety in rhino-sinusal endoscopic surgical procedures.[16–18]

During the last decades, the development of many post-processing techniques and the modulation of the image presets have allowed for subject- and condition-based interpretations of magnetic resonance imaging (MRI),[19–41] ultrasonography[42] and computed tomography (CT) data,[43–45] thus providing the real 3D morphology of several structures and better highlighting anatomical details. In this regard, the direct volume rendering (DVR) is a direct technique to visualize primitive volumes without any intermediate conversion of the volume data to surface presentation.[46]

However, despite its clinical usefulness, to the best of our knowledge, only a few 3D-reconstruction studies have demonstrated the course of the AEA and its relationship with the skull base and adjacent structures through non-invasive imaging in living human subjects.[47,48]

Based on these simple premises, the present work is aimed at i) visualizing topographic anatomical details, such as the AEA course and its relations with the skull base; ii) understanding whether preoperative detailed information on the course of the AEA in its AEC or its possible dehiscence can be achieved non-invasively and on living human subjects by direct volume rendering (DVR) on multidetector computed tomography (MDCT) with contrast medium of supra aortic trunks (SAT).

Materials and Methods

Participants

We retrospectively evaluated 18 patients, 10 of whom were male and 8 female, aged between 28 and 82 years old (63.4 ± 17.9), who underwent MDCT of the SAT because of suspected cerebral aneurism between the 2015 and 2016.

Data Acquisition

In all patients, MDCT of the cranium was performed by a 64-banks multislice CT scanner Philips MX-8000 EXP v25 model (Philips Medical Systems, New Hartford, CT, USA) with axial volumetric acquisition and with transfemoral infusion of contrast medium (iopromide) at a dose of 120 mg/ml.

We evaluated the lengths and distances between the AEA at its entry point in the nasal cavity and the skull base, the middle portion of the frontal beak and the head of middle turbinate on all patients (►**Fig. 1**).

Direct Volume Rendering

A 3D reconstruction was performed by using a freeware graphic software package Osirix 3.3.1, 64-bit (Pixmeo SARL, Geneva, Switzerland). The reconstruction was performed with fields of view of 21×21cm, with the result that the voxel size of the in-plane became 0.41×0.41 mm with a 512×512 matrix. Once the CT scan was acquired, the data were sent to the workstation Apple Mac Pro 2.7 GHz 12-Core Intel Xeon E5 equipped with 64 GB 1866 MHz DDR3 RAM and AMD FirePro D500 3072 graphics, where the images were viewed as consecutive axial sections and analyzed by using the Osirix 3.3.1 software (Pixmeo SARL).

A voxel-intensity histogram was created, and then a transfer function, in the form of a window level, mapped each voxel in the histogram for color and opacity. The voxel positioned under the ramp of function was displayed with a color scale to reflect the volume averaging of different tissue types.[49,50] The brightness and opacity of the voxels have been

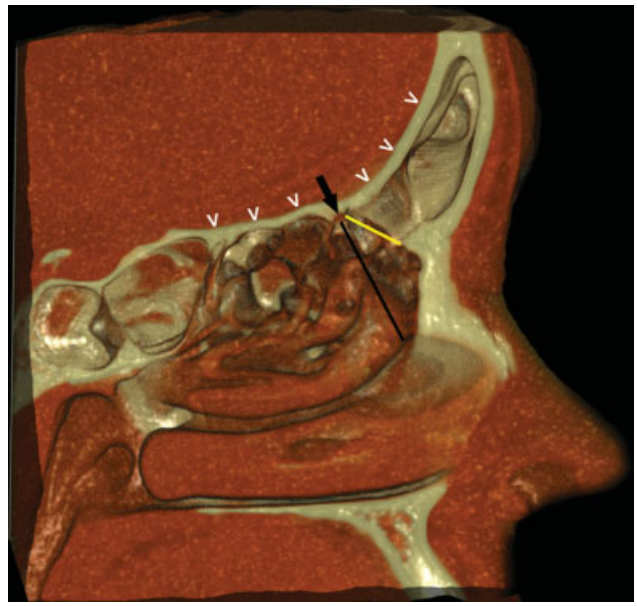

Fig. 1 Distance between the anterior ethmoidal artery and topographical reference points. Paramedian sagittal section. Black arrows show the entry point of the anterior ethmoidal artery in the nasal cavity; its distance from the frontal beak (yellow line) and from the anterior limit of the middle turbinate (black line) are also shown.

regulated by increasing or decreasing them with up-regulation of the transfer function height.

Decreasing and increasing the window level permitted to display higher or lower attenuation structures so that the final image comprises the pixels of interest. Indeed, we were able to modulate the final image working on the window's width and level, to create the 3D image; the final image was adjusted at the workstation to choose, selectively, the structure to highlight (i.e., vessels, muscle, or bones) and to increase the conspicuity of the selected tissue, maintaining, at the same time, the vascular 3D relationships.

Through a process of digitization and interpolation, it was possible to enlarge and/or shrink, translate, and rotate the 3D image.

The Mann-Whitney U test was used to assess differences in measurements between the genders and the sides. A 95% of confidence level was considered, and the statistical significance was set at $p < 0.05$.

Results

The topographical location of 36 AEAs was assessed in vivo in a total of 18 patients.

We evaluated the lengths and distances of the AEA from the skull base, from the middle portion of the frontal beak and from the head of the middle turbinate (►**Fig. 1**). Statistical analysis reported no significant differences between the left and right sides (►**Table 1**) nor gender-related variations (►**Table 2**).

Relations between the AEA and its bony canal were assessed: 10 AEAs (27.8%) were found to be dehiscent, 20 (55.5%) were intracanal, and, in 6 cases (16.7%), the AEC was incomplete and open antero-inferiorly and the arteries were strictly adherent to the skull base.

Fig. 2 Axial plane of the skull base as obtained by means of direct volume rendering. The section is conducted at the level of the frontal sinus. The large wing of the sphenoid, the ethmoid, the crista galli, and a section of the frontal bone can be observed. The arrows show different anatomical structures as they are clearly represented and distinguished by means of the volume rendering: vascular structures arteries of the circle of Willis (white arrow), muscular structures, ocular recti muscles lateral rectus (green arrow), medial rectus (gray arrow), optic nerves (cyan arrow), eyeballs (yellow arrow), brain parenchyma (blue arrow) and skull (magenta).

Applying the algorithm of DVR and extracting the isosurface on a transverse plane, we obtained a three-dimensional image (►**Fig. 2**) in which it was possible to distinguish the bone, the vascular, muscular and connective structures, as well as cavity spaces.

Table 1 Quantitative data on the length of the anterior ethmoidal artery and its distance from important anatomical landmarks (comparison between the left and right sides). No significant differences emerged. Mean values are expressed in millimeters (mm)

	Left mean ± SD	Right mean ± SD	*p* Mann-Whitney U test
Anterior ethmoidal artery length	4.75 ± 2.26	5.13 ± 2.29	0.73
Distance from the head of the middle concha	24.35 ± 4.80	25.55 ± 3.95	0.60
Distance from the skull base	2.64 ± 2.54	2.51 ± 2.54	0.76
Distance from the frontal beak	13.06 ± 2.33	12.94 ± 2.73	0.95

Abbreviation: SD, standard deviation.

Table 2 Quantitative data on the length of the anterior ethmoidal artery and its distance from important anatomical landmarks (comparison between male and female subjects). No significant differences were found. Mean values are expressed in millimeters (mm)

	Female mean ± SD	Male mean ± SD	*p* Mann-Whitney U test
Anterior ethmoidal artery length	4.30 ± 2.42	5.75 ± 1.75	0.10
Distance from the head of the middle concha	24 ± 2.99	26.15 ± 5.54	0.45
Distance from the skull base	2.35 ± 2.60	2.86 ± 2.44	0.62
Distance from the frontal beak	13.54 ± 2.46	12.33 ± 2.45	0.37

Abbreviation: SD, standard deviation.

Zooming on the transverse plane at the ethmoidal level, it was possible to obtain a better visibility of the AEA and AEC.

The two AECs, from the medial wall of the orbit (lamina papiracea), reached the lateral portion of the lamina cribrosa; they moved to the neurovascular peduncle, including the artery, the vein, and the anterior ethmoidal nerve. In ►**Fig. 3**, the CT and 3D DVR images are compared.

By navigating through the skull base, modulating the parameters of intensity, opacity and transparency, mitigating the bone and amplifying the vascular signal, it was possible to better highlight the vascular structures, as depicted in ►**Fig. 4**. The magnification shows the origin of the AEA from the ophthalmic artery to its end at the level of the lamina cribrosa, where it becomes the anterior meningeal artery. (►**Fig. 5**).

Discussion

The AEA originates from the ophthalmic artery within the orbital cavity, moves to the nasal cavity through the anterior ethmoidal foramen, and crosses antero-medially the ethmoidal sinus to reach the cribriform plate.

The identification of the AEA during an ethmoidectomy is of major importance to better detect the fronto-ethmoidal recess, which is always separated from the first ethmoidal foveola. The AEA is closely related to the ethmoidal fovea, and where the ethmoidal fovea inserts at the skull base, the lateral lamella of the cribriform plate (the thinnest bone in the skull base) can be found.[51] This is the point of highest surgical risk.[52] Several methods have been proposed to identify the AEC: Kirchner et al, in 1961,[53] used the maxillo-lacrimal suture, while Lang[54] suggested the cribriform

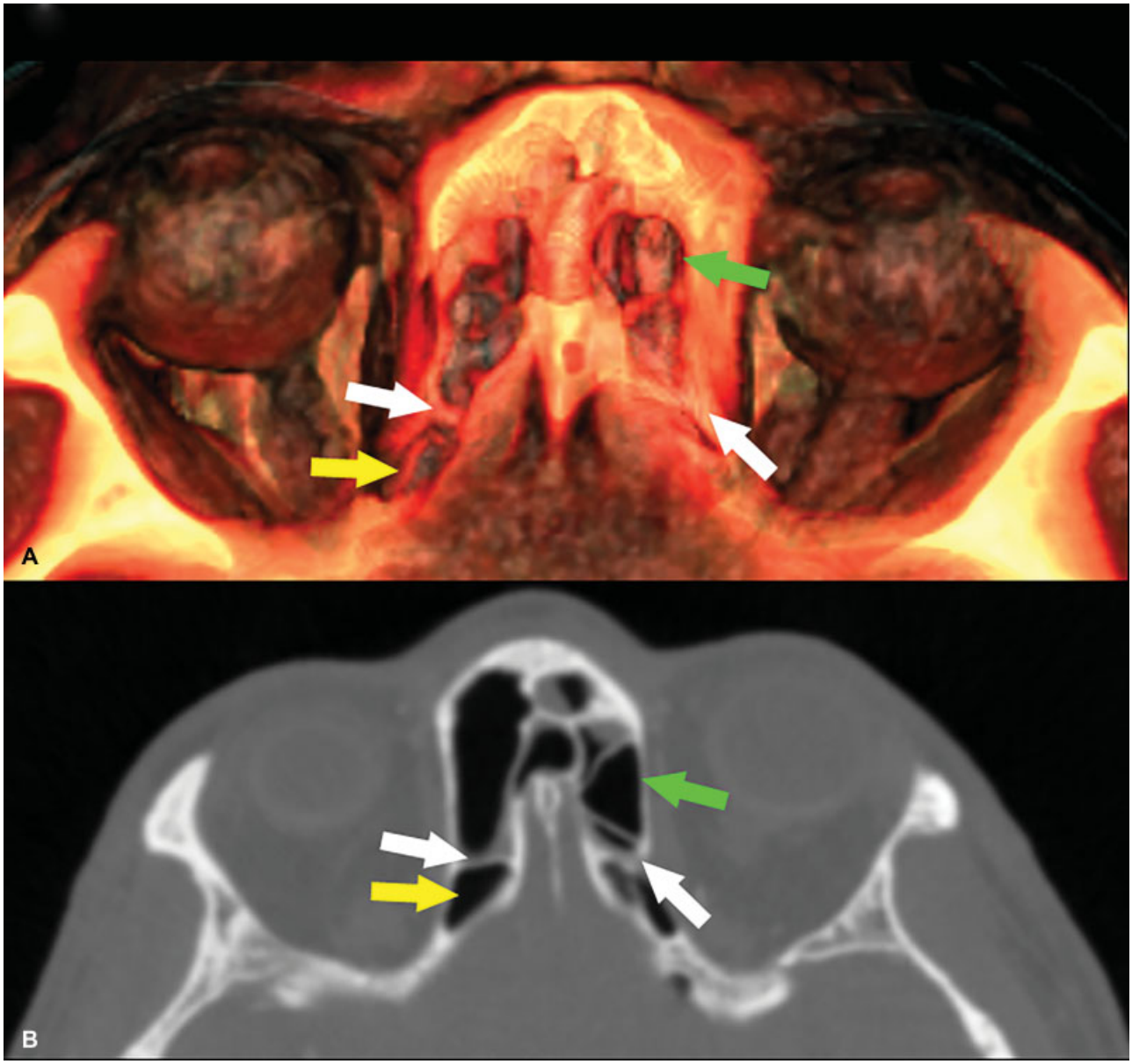

Fig. 3 **Comparison between the same image as obtained by means of 3D direct volume rendering (A) and computed tomography (B).** In the axial plane, the anterior ethmoidal artery (white arrows), the frontal sinuses (green arrows), and the supraorbital recesses (yellow arrows) are visible.

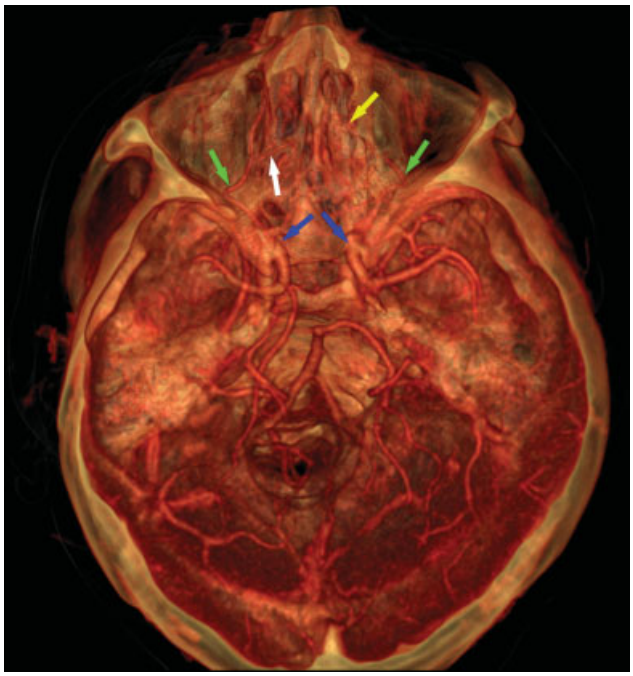

Fig. 4 Axial section of the skull after modulation of intensity and transparency parameters and amplification of the vascular signal to better visualize the vascular structures. The image shows: the internal carotid arteries (blue arrows), the ophthalmic arteries (green arrow), left anterior ethmoidal artery (AEA) (white arrow), right AEA (yellow arrow). As clearly demonstrated by the image, in this patient, the left AEA was extracanal, while the right AEA is intracanal, within the AEC.

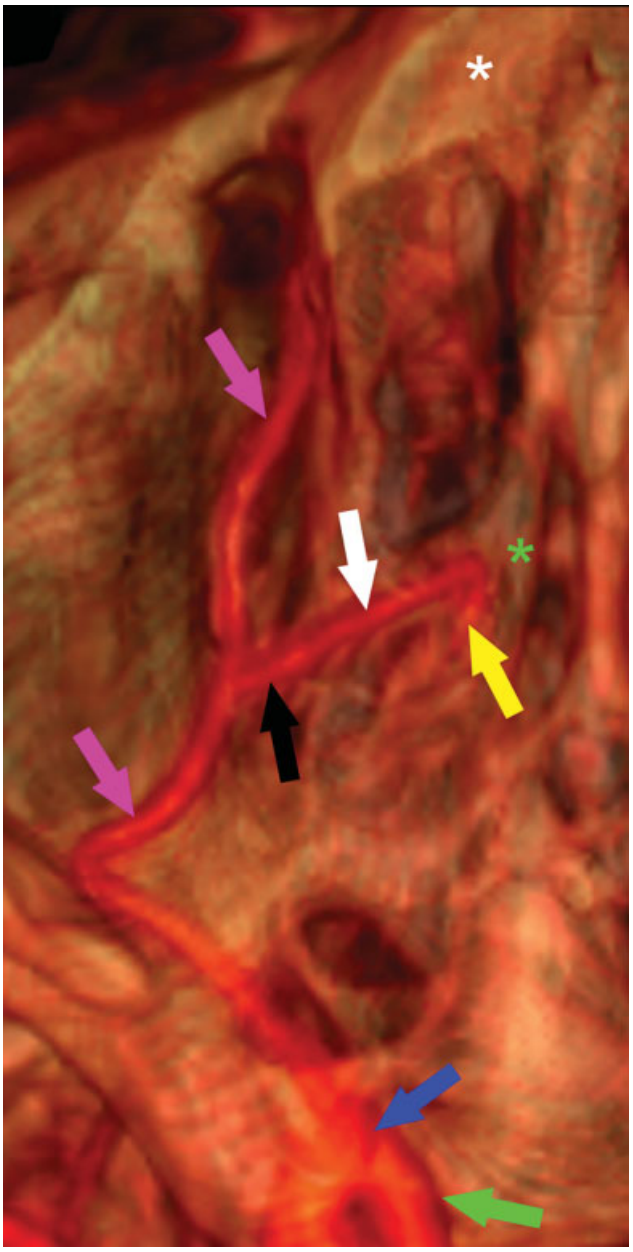

Fig. 5 A more detailed axial section allows to show the complete course of the left anterior ethmoidal artery. The anterior ethmoidal artery (white arrow) originates from the ophthalmic artery (cyan arrow) in an advanced point of its path, between the exit from the carotid siphon (green arrow) and the terminal branches in the anterior wall of the frontal bone (white asterisk); then, it goes along its intraorbital tract (black arrow), passes the lamina papyracea, and then becomes intranasal (white arrow). At the level of the lamina cribrosa (green asterisk), it turns back and becomes the anterior falx artery (yellow arrow).

plate as a landmark. However, these attempts to search for points of landmarks are difficult to accomplish during ESS (i.e., Araujo Filho studied the distance between the AEA and the anterior nasal spine).[1]

In 1988, Kainz and Stammberger described the AEA with an upturned half-moon shape resting on the skull base and with an average width of ~ 5 mm.[55] Recent CT and dissection studies assessed the localization of the AEA between the second and third lamella in 87.1% of the cases, while in the remaining 12.9% it was inside the 2nd or the 3rd lamella; in no cases the AEA emerged anterior to the bulla ethmoidalis.[3] Moreover, in some cases, the AEC may be incomplete or even absent, thus exposing the artery to direct trauma.[3,56]

Several variations of the AEA have been previously described. Simmen et al evaluated 34 cadaver heads, showing that the AEAs were located in the retrobullar recess or roof of the bulla ethmoidalis (14.7%) and in the recess between the 2nd and 3rd lamella (85.3%).[4] Yang et al studied 15 cadavers and found that 85% of the AEAs were posterior to the bulla ethmoidalis, 10.7% were in the roof of the frontal recess, and 3.6% were in the roof of the posterior ethmoid sinus.[57]

During the last decade, consistent effort has been made to allow for a reliable pre- and/or intraoperatory identification of the AEA, either by using anatomy and topographic landmarks[1,4,14,58–61] or imaging techniques. To date, three-dimensional spin digital subtraction angiography (DSA) is the gold standard for preoperative assessment of anatomy and relations of the AEA and the AEC.[48] Many CT scans, both on cadavers and on living patients, have been performed to identify the AEA and assess its course.[4,59,60,62–67]

►**Table 3** summarizes the most important findings of the last decade.

However, the AEA may be difficult to identify, especially in the presence of pathologies, on CT scan because of the morphological and structural complexity of this anatomical region that may lead to several issues. In patients with chronic sinusitis or polyposis, Pandolfo et al[47] were able to

Table 3 Summary of the studies of the last decade on the assessment of the anterior ethmoidal artery

Authors	Year	Patients	Controls	Techniques	Results
Yenigun et al	2016	184 CT scans, excluding patients with nasal polyposis, sinus anomalies, previous sinus surgery.		CT scans	Positive correlation between the AEC, the superior–inferior depth of the lateral lamella of the cribriform plate LLCP, and the anterior–posterior length.
Wong et al	2014	1 Waardenburg syndrome and chronic rhinosinusitis	–	CT scan	The AEA was not identified on preoperative CT. Intraoperatively, the AEA was found to be anterior to the bulla ethmoidalis, within the frontal recess, and was inadvertently injured.
Ding et al	2012	32 (30 intracranial aneurisms, 2 meningiomas)	–	3D spin DSA; 320-slice CTA	The entire course of the AEA was seen in 100% (32) of the cases with 3D spine DSA and in 29 of 32 cases (90.1%) with 320-slice CTA, with no significant difference.
Monjas-Cánovas et al	2011	–	20 cadavers	CT scan; MIP	AEA identified in 95% (38/40) of the scans. Mean length of the anterior ethmoidal canal: 8.43 ± 0.74 mm. The angle performed into the skull base was 37.3 ± 5.48 degrees. Topographical location: between the second and third lamella in 90% of the cases (36/40).
Joshi et al	2010	–	50	CT scan	AEA identified in 97% of the scans. Mean distance between artery and skull base: 1.5 mm in absence of the supraorbital cell; 4.86 mm in the presence of the supraorbital cell.
Yang et al	2009	–	15 randomly selected adult cadavers	Dissection	Average diameter of the AEA: 0.80 ± 0.24 mm. Topographical location: between the second and third lamella in 87.5% of the cases; over the roof of the frontal recess cells in 10.7%; over the roof of the posterior ethmoid sinus in 3.6%. The angle formed by the long axis of the artery and the lamina papyracea was 60.5 ± 16.4 degrees.
Souza et al	2009	198 CT scans of patients excluding: patients aged below 12 years, a history of surgery or trauma in the paranasal sinuses or the skull base, congenital anomalies of the face, paranasal sinus malignancies, osteofibrous lesions, sinus diseases.	–	CT scan	AEC identified in 41% of the scans. Anterior ethmoidal sulcus identified in 98% of the scans; anterior ethmoidal foramen identified in 100% of scans.
Han et al	2008	–	24 cadaver heads	Dissection	Mean distance from the axilla: 17.5 mm. Mean distance from the posterior ethmoid artery: 14.9 mm Topographical location: anterior to 31%, at 36%, or immediately posterior to 33% the superior attachment of the basal lamella.
McDonald et al	2008		50	CT scan	Anterior ethmoidal foramen identified in 95% of the cases bilaterally and in the remaining 5% unilaterally. AEA identified in 33% of the scans.
Riehm et al	2008	–	9 cadavers	Dissection, CT scans	Correlation between CT and surgical findings allowed identification of 2 criteria predictive of AEA origin: 1 presence of an ethmoid bulla above the AE C2 AEC located below the ethmoid roof, anterior to the bulla.
Pandolfo et al	2007	20 18 subarachnoid hemorrhage, 2 meningiomas	78 (25 chronic sinusitis, 40 massive poliposis, 13 cases of single polyp	Dual volume angiography and MDCT patients; MDCT controls	On patients, the entire course of the AEA was identified by means of DVA angiography: AEA behind the frontal recess (18/20); AEA near to the posterior wall of frontal recess 2/20. On controls, MDCT only (110/156) AEAs were identified only indirectly; 46 out of 156 were shown in their entirety.
Lannoy-Penisson et al	2007		9 heads	Dissection, CT scan	The arteries were identifiable on CT scans. Topographical location: arteries were included in the roof of the ethmoid in 8 cases; prominent under the roof in 3 cases; distant from the roof in 7 cases, in association with pneumatization of the floor of the orbit.
Erdogmus et al	2006	–	19 adult cadavers	Dissection	The AEA was observed in all specimens except for one case. Average diameter: 92 +/− 0.2 mm on the right and 0.88 +/− 0.15 mm on the left. Four variations of its course were differentiated and described.
Floreani et al	2006	–	22 cadaver heads	CT scan	AEA unable to be clipped in 66% of the cases; clipped effectively, all in a mesentery in 20% of cases; not effectively clipped in 14%.
Araujo Filho et al	2006	–	25 cadavers with no past nasosinusal injury/surgery and altered anatomy	Dissection	Average intranasal length of the AEA: 5.2 mm. AEC dehiscence in 66.7%. Average distance between the artery middle point to the anterior nasal spine: 61.72 mm. Average distance from the nasal axilla: 64.04 mm. Average distance from the anterior axilla to the middle turbinate:21.14 mm.

Abbreviations: AE, ; AEA, anterior ethmoidal artery; AEC; anterior ethmoidal canal; CTA, computed-tomography angiography; DSA, digital subtraction angiography; DVA, dynamic volumetric angiography; LLCP, lateral lamella of the cribriform plate; MDCT, multidetector computed tomography; MIP, maximum intensity projection.

identify the AEA in its entirety only in 23 of 78 patients (46 AEA); McDonald and colleagues successfully identified the AEA only in 33% of the CT scans[62]; Souza et al[63] were able to find the AEC only in 41% of the exams; finally, an anatomical variation of the AEA course, described by Wong et al[67] in a case study of a patient with Waanderburg Syndrome and chronic rhinosinusitis, was not detected in preoperative CT and then injured during the surgery.

Taking into account the aforementioned limitations, we applied the 3D-DVR technique to evaluate the quantitative and qualitative features of the AEA and its relations with the skull base and neighboring structures. Taken together, our results show that 3D-DVR is a useful technique for a detailed characterization of the localization and anatomical relationships of the AEA.

Conclusion

In conclusion, we showed the 3D reconstruction of the AEA in its entirety and topographic complexity. However, further studies are needed to assess the usefulness of in vivo CT-based 3D volume rendering as a tool for preoperative assessment. Nevertheless, we would like to stress the great potential of this technique for visualization purposes, ranging from clinical evaluations to anatomical studies or even educational images.

What has been pursued and achieved is summarized in the perception of anatomical, morphological and topographic detail in a new tridimensional framework, which gives added value to any physician, no matter his/her area of specialization, from surgery to radiology, from anatomy to clinic.

Conflicts of Interest

The authors report that there are no conflicts of interest.

References

1 Araujo Filho BC, Weber R, Pinheiro Neto CD, Lessa MM, Voegels RL, Butugan O. Endoscopic Anatomy of the anterior ethmoidal artery: a cadaveric dissection study. Rev Bras Otorinolaringol 2006; 72:323–328

2 Pollok JS, Newton TH. The anterior falx artery: normal and pathologic anatomy. Radiology 1968;91:1089–1095

3 Moon HJ, Kim HU, Lee JG. Surgical anatomy of the anterior ethmoidal canal in ethmoid roof. Laryngoscope 2001;111:900–904

4 Simmen D, Raghavan U. The surgeon's view of the anterior ethmoidal artery. Clin otolaryngol 2006;31:187–191

5 Floreani SR, Nair SB, Switajewski MC, Wormald PJ. Endoscopic anterior ethmoidal artery ligation: a cadaver study. Laryngoscope 2006;6:1263–1267

6 Xiang YY, Xu DC, Huang FL, Zhang XK. Applied anatomy of the ligation of ethmoidal artery with nasal endoscope. Chin J Clin Anat 2002;20:375–376

7 Lee WC, Ming Ku PK, Van Hasselt CA. New guidelines for endoscopic localization of the anterior ethmoidal artery: a cadaveric study. Laryngoscope 2000;110:1173–1178

8 Mafee MF, Chow JM, Meyers R. Functional endoscopic sinus surgery: anatomy, CT screening, indications: complications. Am J Roentgenol 1993;160:735–744

9 Ohnishi T, Yanagisawa E. Endoscopic anatomy of the anterior ethmoidal artery. Ear Nose Throat J 1994;73(09):634–636

10 Mafee MF. Preoperative imaging anatomy of the nasal complex for functional endoscopic sinus surgery. Radiol Clin North Am 1993; 31:1–2

11 Akdemir G, Tekdemir I, Altin L. Transethmoidal approach to the optic canal: surgical and radiological microanatomy. Surg Neurol 2004;623:1–6

12 Gotwald TF, Menzler A, Beauchamp NJ, ZurNedden D, Zinreich SJ. Paranasal and orbit anatomy revisited: identification of the ethmoid arteries on coronal CT scans. Crit Rev ComputTomogr 2003;44:263–278

13 Cassano M, Longo M, Fiocca-Matthews E, Del Giudice AM. Endoscopic intraoperative control of epistaxis in nasal surgery. Auris Nasus Larynx 2010;37:178–184

14 Rudmik L, Smith TL. Management of intractable spontaneous epistaxis. Am J Rhinol Allergy 2012;26(01):55–60

15 Yang BDYX, Lu QK. Morphological characteristics of the Anterior Ethmoidal Artery in Ethmoid Roof and Endoscopic localization. Skull base 2009;19:311–318

16 Asanau A, Timoshenko AP, Vercherin P, Marthin C, Prades JM. Sphenopalatine and anterior ethmoidal artery ligation for severe epistaxis. Ann Otol Rhinol Laryngol 2009;118:639–644

17 Galletti B, Gazia F, Freni F, Sireci F, Galletti F. Endoscopic sinus surgery with and without computer assisted navigation: A retrospective study. Auris Nasus Larynx 2019;46(04):520–525

18 McMains KC. Safety in endoscopic sinus surgery. Curr Opin Otolaryngol Head Neck Surg 2008;163:247–251

19 Ciodaro F, Mannella VK, Nicita RA, Cammaroto G, Bruno R, Galletti B, Freni F, Galletti F. Therapeutic efficacy of the Galletti-Contrino manoeuvre for benign paroxysmal positional vertigo of vertical semicircular canals in overweight subjects. Eur Arch Otorhinolaryngol 2018;275(10):2449–2455

20 Cacciola A, Milardi D, Bertino S, Basile GA, Calamuneri A, Chillemi G, Rizzo G, Anastasi G, Quartarone A. Structural connectivity-based topography of the human globus pallidus: Implications for therapeutic targeting in movement disorders. Mov Disord 2019; 34:987–996

21 Cacciola A, Milardi D, Basile GA, Bertino S, Calamuneri A, Chillemi G, et al. The cortico-rubral and cerebello-rubral pathways are topographically organized within the human red nucleus. Sci Rep 2019;9(01):1–12

22 Cacciola A, Milardi D, Quartarone A. Role of cortico-pallidal connectivity in the pathophysiology of dystonia. Brain 2016;139:48

23 Cacciola A, Milardi D, Anastasi GP, Basile GA, Ciolli P, Irrera M, Cutroneo G, Bruschetta D, Rizzo G, Mondello S, Bramanti P, Quartarone A. A Direct Cortico-Nigral Pathway as Revealed by Constrained Spherical Deconvolution Tractography in Humans. Front Hum Neurosci 2014;10:374

24 Cacciola A, Milardi D, Calamuneri A, Bonanno L, Marino S, Ciolli P, Russo M, Bruschetta D, Duca A, Trimarchi F, Quartarone A, Anastasi G. Constrained Spherical Deconvolution Tractography Reveals Cerebello-Mammillary Connections in Humans. Cerebellum 2017;16(02):483–495

25 Cacciola A, Milardi D, Livrea P, Flace P, Anastasi G, Quartarone A. The Known and Missing Links Between the Cerebellum, Basal Ganglia, and Cerebral Cortex. Cerebellum 2017;16(03):753–755

26 Cacciola A, Calamuneri A, Milardi D, Mormina E, Chillemi G, Marino S, Naro A, Rizzo G, Anastasi G, Quartarone A. A Connectomic Analysis of the Human Basal Ganglia Network. Front Neuroanat 2017;11:85

27 Cacciola A, Calabrò RS, Costa A, Naro A, Milardi D, Bruschetta D. Enlarged Virchow-Robin Spaces in A Young Man: A Constrained Spherical Deconvolution Tractography Study. Acta Biomed 2017; 88:319–324

28 Milardi D, Arrigo A, Anastasi G, Cacciola A, Marino S, Mormina E, Calamuneri A, Bruschetta D, Cutroneo G, Trimarchi F, Quartarone A. Extensive Direct Subcortical Cerebellum-Basal Ganglia Connections in Human Brain as Revealed by Constrained Spherical Deconvolution Tractography. Front Neuroanat 2016;18(10):29

29 Milardi D, Cacciola A, Cutroneo G, Marino S, Irrera M, Cacciola G, Santoro G, Ciolli P, Anastasi G, Calabrò RS, Quartarone A. Red nucleus connectivity as revealed by constrained spherical deconvolution tractography. Neurosci Lett 2016;626:68–73

30 Milardi D, Cacciola A, Calamuneri A, Ghilardi MF, Caminiti F, Cascio F, Andronaco V, Anastasi G, Mormina E, Arrigo A, Bruschetta D, Quartarone A. The Olfactory System Revealed: Non-Invasive Mapping by using Constrained Spherical Deconvolution Tractography in Healthy Humans. Front Neuroanat 2017;10:11–32

31 Russo M, Calamuneri A, Cacciola A, Bonanno L, Naro A, Dattola V, Sessa E, Buccafusca M, Milardi D, Bramanti P, Calabrò RS, Quartarone A. Neural correlates of fatigue in multiple sclerosis: a combined neurophysiological and neuroimaging approach (R1). Arch Ital Biol 2017;155(03):142–151

32 Portaro S, Filardi V, Naro A, Cacciola A, Andronaco V, Gatani U, Calabrò RS, Gemelli G, Milardi D, Bramanti A. Force and strain during horseback riding :bridging the gap between theory and clinical practice. J Sports Med Phys Fitness 2019;59(03):536–538. doi: 10.23736/S0022-4707.18.08170-7. Epub 2018 Sep 27. PubMed PMID: 30264970

33 Naro A, Calabrò RS, Leo A, Russo M, Milardi D, Cannavò A, Manuli A, Buda A, Casella C, Bramanti P, Cacciola A, Bramanti A. Bridging the Gap Towards Awareness Detection in Disorders of Consciousness: An Experimental Study on the Mirror Neuron System. Brain Topogr 2018;31(04):623–639. doi: 10.1007/s10548-018-0628-9. Epub 2018 Feb 7. PubMed PMID: 29417320

34 Naro A, Milardi D, Cacciola A, Russo M, Sciarrone F, La Rosa G, Bramanti A, Bramanti P, Calabrò RS. What Do We Know About the Influence of the Cerebellum on Walking Ability? Promising Findings from Transcranial Alternating Current Stimulation. Cerebellum 2017;16(04):859–867. doi: 10.1007/s12311-017-0859-4. PubMed PMID: 28456901

35 Leonardi S, Cacciola A, De Luca R, Aragona B, Andronaco V, Milardi D, Bramanti P, Calabrò RS. The role of music therapy in rehabilitation: improving aphasia and beyond. Int J Neurosci 2018;128 (01):90–99. doi: 10.1080/00207454.2017.1353981. Epub 2017 Aug 8. Review. PubMed PMID: 28689476

36 Naro A, Bramanti P, Leo A, Cacciola A, Bramanti A, Manuli A, Calabrò RS. Towards a method to differentiate chronic disorder of consciousness patients' awareness: The Low-Resolution Brain Electromagnetic Tomography Analysis. J Neurol Sci 2016; 368:178–183. doi: 10.1016/j.jns.2016.07.016. Epub 2016 Jul 9. PubMed PMID: 27538628

37 Torrisi M, Cacciola A, Marra A, De Luca R, Bramanti P, Calabrò RS. Inappropriate behaviors and hypersexuality in individuals with dementia: An overview of a neglected issue. Geriatr Gerontol Int 2017;7(06):865–874. doi:10.1111/ggi.12854. Epub 2016 Aug 4. Review. PubMed PMID: 27489168

38 Anastasi G, Cutroneo G, Bruschetta D, Trimarchi F, Ielitro G, Cammaroto S, Duca A, Bramanti P, Favaloro A, Vaccarino G, Milardi D. Three-dimensional volume rendering of the ankle based on magnetic resonance images enables the generation of images comparable to real anatomy. J Anat 2009;215(05):592–599. doi:10.1111/j.1469-7580.2009.01133.x. Epub 2009 Aug 12. PubMed PMID: 19678857; PubMed Central PMCID: PMC2780576

39 Anastasi G, Bramanti P, Di Bella P, Favaloro A, Trimarchi F, Magaudda L, Gaeta M, Scribano E, Bruschetta D, Milardi D. Volume rendering based on magnetic resonance imaging: advances in understanding the three-dimensional anatomy of the human knee. J Anat 2007;211(03):399–406. Epub 2007 Jul 21. PubMed PMID: 17645453; PubMed Central PMCID: PMC2375819

40 Meduri M, Bramanti P, Ielitro G, Favaloro A, Milardi D, Cutroneo G, Muscatello MR, Bruno A, Micò U, Pandolfo G, La Torre D, Vaccarino G, Anastasi G. Morphometrical and morphological analysis of lateral ventricles in schizophrenia patients versus healthy controls. Psychiatry Res 2010;83(01):52–58. doi: 10.1016/j.pscychresns.2010.01.014. Epub 2010 Jun 9. PubMed PMID: 20538436

41 Trimarchi F, Bramanti P, Marino S, Milardi D, Di Mauro D, Ielitro G, Valenti B, Vaccarino G, Milazzo C, Cutroneo G. MRI 3D lateral cerebral ventricles in living humans: morphological and morphometrical age-, gender-related preliminary study. Anat Sci Int 2013;88(02):61–69. doi: 10.1007/s12565-012-0162-x. Epub 2012 Nov 20. PubMed PMID: 23179909

42 Bruschetta D, Milardi D, Trimarchi F, Di Mauro D, Valenti A, Arrigo A, Valenti B, Santoro G, Cascio F, Vaccarino G, Cacciola A. Muscle contracture diagnosis: the role of sonoelastography. J Sports Med Phys Fitness 2016;56:1518–1525

43 Cutroneo G, Bruschetta D, Trimarchi F, Cacciola A, Cinquegrani M, Duca A, Rizzo G, Alati E, Gaeta M, Milardi D. In Vivo CT Direct Volume Rendering: A Three-Dimensional Anatomical Description of the Heart. Pol J Radiol 2016;21(81):21–28

44 Cuccia AM, Caradonna C, Bruschetta D, Vaccarino G, Milardi D. Imaging of temporomandibular joint: approach by direct volume rendering. J Clin Diagn Res 2014;8(11):ZC105-9. doi: 10.7860/JCDR/2014/9977.5195. Epub 2014 Nov 20.PubMed PMID: 25664280; PubMed Central PMCID: PMC4287995

45 Cuccia AM, Caradonna C, Caradonna D, Anastasi G, Milardi D, Favaloro A, De Pietro A, Angileri TM, Caradonna L, Cutroneo G. The arterial blood supply of the temporomandibular joint: an anatomical study and clinical implications. Imaging Sci Dent 2013;43 (01):37–44. doi: 10.5624/isd.2013.43.1.37. Epub 2013 Mar 11. PubMed PMID: 23525363; PubMed Central PMCID: PMC3604369

46 Kaneko T, Yamamoto Y. Volume-preserving surface reconstruction from volume data. Proc IntConf Image Proc 1997;1:145–148

47 Pandolfo I, Vinci S, Salamone I, Granata F, Mazziotti S. Evaluation of the anterior ethmoidal artery by 3D dual volume rotational digital subtraction angiography and native multidetector CT with multiplanar reformations. Initial findings. Eur Radiol 2007;17 (06):1584–1590

48 Ding J, Sun G, Lu Y, Yu BB, Li M, Li L, et al. Evaluation of anterior ethmoidal artery by 320-slice CT angiography with comparison to three-dimensional spin digital subtraction angiography: initial experiences. Korean J Radiol 2012;136:667–673

49 Drebin B, Fishman EK, Magid D, et al. Volumetric rendering techniques: applications for three-dimensional imaging of the hip. Radiology 1987;163:737–738

50 Taubin G. A signal processing approach to fair surface design. Computer Graphics Proceedings 1997; 351

51 Stammberger HR, Kennedy DW, Anatomic Terminology Group. Paranasal sinuses: anatomic terminology and nomenclature. Ann Otol Rhinol Laryngol Suppl 1995;167:7–16

52 Adeel M, Ikram M, Rajput MS, Arain A, Khattak YJ. Asymmetry of lateral lamella of the cribriform plate: a software-based analysis of coronal computed tomography and its clinical relevance in endoscopic sinus surgery. Surg Radiol Anat 2013; 359:843–847

53 Kirchner JA, Yanagisawa E, Crelin Jr ES. Surgical anatomy of the ethmoidal arteries. A laboratory study of 150 orbits. Arch Otolaryngol 1961;74:382–386

54 Lang J, Schäfer K. Ethmoidal arteries: origin, course, regions supplied and anastomoses. Acta Anat Basel 1979;104(02):183–197

55 Kainz J, Stammberger H. The roof of the anterior ethmoid: a locus minoris resistentiae in the skull base. Laryngol Rhinol Otol Stuttg 1988;67(04):142–149

56 Minnigerode B. Zur Anatomie und klinischen Bedeutung des Canalis ethmoidalis. Zeitschrift fur Laryngologie, Rhinologie, Otologie und ihre Grenzgebiete 1966;45:554–559

57 Yang Y, Lu Q, Liao J, Dang R. Morphological Characteristics of the Anterior Ethmoidal Artery in Ethmoid Roof and Endoscopic Localization. Skull Base 2009;19(05):311–317. doi:10.1055/s-0028-1115323

58 Erdogmus S, Govsa F. The anatomic landmarks of ethmoidal arteries for surgical approaches. J Craniofac Surg 2006;17:280–285

59 Lannoy-Penisson L, Schultz P, Riehm S, Atallah I, Veillon F, Debry C. The anterior ethmoidal artery: radio-anatomical comparison and

its application in endonasal surgery. Acta Otolaryngol 2007;127 (06):618–622
60 Riehm S, Pénisson L, Charpiot A, Schultz P, Veillon F, Debry C. CT imaging of the anterior ethmoidal artery: anatomic correlation. J Radiol 2008;89(02):229–233
61 Han JK, Becker SS, Bomeli SR, Gross CW. Endoscopic localization of the anterior and posterior ethmoid arteries. Ann Otol Rhinol Laryngol 2008;117(12):931–935
62 McDonald SE, Robinson PJ, Nunez DA. Radiological anatomy of the anterior ethmoidal artery for functional endoscopic sinus surgery. The Journal of Laryngology & Otology 2008;122(03): 264–267. doi: 10.1017/S0022215107008158
63 Souza SA, Souza MM, Gregório LC, Ajzen S. Anterior ethmoidal artery evaluation on coronal CT scans. Braz J Otorhinolaryngol 2009;75(01):101–106
64 Joshi AA, Shah KD, Bradoo RA. Radiological correlation between the anterior ethmoidal artery and the supraorbital ethmoid cell. Indian J Otolaryngol Head Neck Surg 2010;62(03):299–303
65 Monjas-Cánovas I, García-Garrigós E, Arenas-Jiménez JJ, Abarca-Olivas J, Sánchez-Del Campo F, Gras-Albert JR. Radiological anatomy of the ethmoidal arteries: CT cadaver study. Otorrinolaringol Esp 2011;625:367–374. doi: 10.1016/j.otorri.2011.04.006
66 Yenigun A, Goktas SS, Dogan R, Eren SB, Ozturan O. A study of the anterior ethmoidal artery and a new classification of the ethmoid roof: Yenigun classification. Eur Arch Otorhinolaryngol 2016;273 (11):3759–3764
67 Wong DK, Shao A, Campbell R, Douglas R. Anterior ethmoidal artery emerging anterior to bulla ethmoidalis: An abnormal anatomical variation in Waardenburg's syndrome. Allergy Rhinol Providence 2014;5(03):168–171. doi:10.2500/ar.2014.5.0094